Gain enhancement in a XeC1 pumped Raman amplifier
by Jeffrey Rifkin

A thesis submitted in partial fulfillment of the requirements for the degree of Master of Science in Physics
Montana State University

Abstract:
Gain enhancement in an excimer-pumped Raman amplifier consisting of molecular hydrogen is experimentally measured. Gain enhancement is measured both as a function of optical delay and input pump intensity, and in the two limits when the laser mode spacing is large, and comparable to the linewidth associated with the Raman medium. Experimental results are compared with the predictions of a transient multimode theory. This theory is based on the coupled equations of Raman scattering which describe the transient growth of the Stokes field and coherence of the Stokes transition. A sum over longitudinal modes with fixed and totally random phases is assumed for both the pump laser and Stokes fields.

The theory compares well with experiment in the regime where the Raman linewidth is large compared to the modespacing of the laser. The theory also makes the interesting prediction that in this limit, the broadband gain will be larger than the gain for a narrowband laser.

GAIN ENHANCEMENT IN A XeCl PUMPED RAMAN AMPLIFIER

by

Jeffrey Rifkin

A thesis submitted in partial fulfillment
of the requirements for the degree

of

Master of Science

in

Physics

MONTANA STATE UNIVERSITY
Bozeman, Montana

December 1987

APPROVAL

of a thesis submitted by

Jeffrey Rifkin

This thesis has been read by each member of the thesis committee and has been found to be satisfactory regarding content, English usage, format, citations, bibliographic style, and consistency, and is ready for submission to the College of Graduate Studies.

12-9-87
Date

Chairperson, Graduate Committee

Approved for the Major Department

12-9-87
Date

Head, Major Department

Approved for the College of Graduate Studies

12-11-87
Date

Graduate Dean

STATEMENT OF PERMISSION TO USE

In presenting this thesis in partial fulfillment of the requirements for a master's degree at Montana State University, I agree that the Library shall make it available to borrowers under rules of the Library. Brief quotations from this thesis are allowable without special permission provided that accurate acknowledgment of source is made.

Permission for extensive quotation from or reproduction of this thesis may be granted by my major professor, or in his absence, by the Director of Libraries when, in the opinion of either, the proposed use of the material is for scholarly purposes. Any copying or use of the material in this thesis for financial gain shall not be allowed without my written permission.

Signature 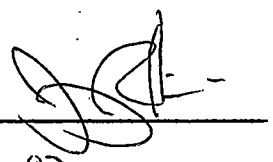

Date 12-9-87

ACKNOWLEDGEMENTS

The author wishes to extend his deepest gratitude to the entire Secretarial staff at the Physics Department of Montana State University. Without their help, this document would never have seen print.

The author would also like to thank his committee members Dr. R. T. Robiscoe and Dr. J. E. Drumheller who read carefully through this thesis and offered many suggestions about how it might be improved. Dave MacPherson also deserves thanks. His patient advice, and physical insight helped unravel mysteries, too many in number to count.

The author is especially grateful to his advisor, Dr. J. L. Carlsten, who was a constant source of inspiration and a model of excellent leadership and management. Dr. Carlsten provided an environment where even the weakest of students could inevitably excel and the author considers himself fortunate indeed for the opportunity to participate.

TABLE OF CONTENTS

	Page
1. INTRODUCTION	1
2. DERIVATION OF THE RAMAN SCATTERING EQUATIONS	5
Introduction	5
Response of the Medium	8
Response of the Field	12
3. ACCOUTERMENTS	17
Equipment and Technique	17
The Laser	21
The Medium	31
4. THEORY	37
Physics	37
Computer Model	39
5. EXPERIMENTS	46
Gain Enhancement	46
Measurement of Beam Profiles	48
Measurement of Zero of Optical Delay	49
6. EXPERIMENTAL RESULTS	51
General Results	51
Gain Enhancement at 100 Atmospheres	54
Zero of Optical Delay	55
Gain Enhancement at 10 Atmospheres	57
7. COMPARISON WITH THEORY	61
Introduction	61
100 Atmospheres	64
10 Atmospheres	67
8. CONCLUSIONS	71
REFERENCES CITED	73

TABLE OF CONTENTS--Continued

Page

APPENDICES..... 78

Appendix A - Relative Size of ΔL..... 79
Appendix B - Transformation to the Travelling Reference Frame..... 81
Appendix C - Computer Programs..... 84

LIST OF FIGURES

Figure		Page
1.	Energy level diagram for stimulated Raman scattering.....	6
2.	Self consistency diagram.....	7
3.	Schematic of experiment to measure magnification of 10cm lens.....	19
4.	Digitized plot of the results of the magnification experiment.....	20
5.	(a) schematic of the XeCl laser and (b) an energy level diagram of the XeCl bond.....	22
6.	Digitized plot of a spectrograph showing the spectral lines of the XeCl laser.....	24
7.	Temporal profile of a typical laser pulse.....	26
8.	Schematic of the Mach-Zehnder interferometer used to measure the laser and Stokes linewidths.....	27
9.	Interferogram made with the Mach Zehnder interferometer and a least squares fit to the data.....	29
10.	Autocorrelation function for (a) the Stokes, (b) the pump and an exponential fit to the data..	30
11.	Schematic of experiment to check for diffraction limited operation of the XeCl laser.....	32
12.	Superposition of the theoretical profile for a diffraction limited beam at focus and the spatial profile of the focused XeCl beam.....	33
13.	Energy level diagram for H_2.....	35
14.	Comparison of experimental and theoretical values for gain enhancement as a function of optical delay.....	41

LIST OF FIGURES--CONTINUED

Figure		Page
15.	Comparison of experimental and theoretical values for correlated and uncorrelated gain enhancement as a function of input pump energy.....	42
16.	Flow chart for the program Mode.....	43
17.	Schematic of the gain enhancement experiment.....	47
18.	Schematic of experiment to measure zero of optical delay.....	50
19.	Profile of Stokes beam through the amplifier cell.....	52
20.	Profile of pump beam through the amplifier cell.....	53
21.	Experimental data for the autocorrelation function used to determine the point of zero delay from the zero of optical delay experiment.....	56
22.	Gain enhancement profile used to determine the location of the enhancement peak from the experiment to measure zero of optical delay.....	58
23.	Experimental and theoretical results for gain enhancement as a function of input pump energy at 10 atmospheres.....	60
24.	Theoretical comparison showing the relative size and spacing of the laser modes and the Raman linewidth.....	62
25.	Theoretical comparison of size of the laser bandwidth and the Raman linewidth.....	63
26.	Plot of the intensity of the theoretically calculated laser field resulting from the superposition of 640 modes.....	65

LIST OF FIGURES--CONTINUED

Figure		Page
27.	Superposition of the traveling and laboratory reference frames	82
28.	Computer program Lfields	85
29.	Computer program Mode	89

ABSTRACT

Gain enhancement in an excimer-pumped Raman amplifier consisting of molecular hydrogen is experimentally measured. Gain enhancement is measured both as a function of optical delay and input pump intensity, and in the two limits when the laser modespacing is large, and comparable to the linewidth associated with the Raman medium.

Experimental results are compared with the predictions of a transient multimode theory. This theory is based on the coupled equations of Raman scattering which describe the transient growth of the Stokes field and coherence of the Stokes transition. A sum over longitudinal modes with fixed and totally random phases is assumed for both the pump laser and Stokes fields.

The theory compares well with experiment in the regime where the Raman linewidth is large compared to the modespacing of the laser. The theory also makes the interesting prediction that in this limit, the broadband gain will be larger than the gain for a narrowband laser.

CHAPTER ONE

INTRODUCTION

Raman scattering was first observed in 1928 by C.V. Raman[1]. A Raman medium is defined as a medium capable of coupling optical frequencies which differ by a vibrational, rotational, or electronic frequency. Raman scattered light is referred to as either Stokes or anti-Stokes radiation[2] depending upon whether the coupling downshifts or upshifts the frequency of the scattered light.

The laser or pump used for Raman scattering can be categorized in one of two ways, either narrowband (monochromatic) or broadband. Numerous models exist to describe the broadband pump. The three most common are the phase diffusion, chaotic, and multimode models. These models all describe the pump as a broadband wave with either fluctuations in amplitude and/or fluctuations in phase. The phase diffusion model[3] assumes constant amplitude with randomly fluctuating phases, e.g. $\mathbf{E}(t)=E\cos(\omega t-kz+\phi(t))$, where E is the amplitude and ϕ is the phase. The chaotic model[4] assumes both randomly fluctuating amplitudes and phases, e.g. $\mathbf{E}(t)=E(t)\cos(\omega t-kz+\phi(t))$, while the multimode model[4] uses a distribution of widely separated modes, fixed in both amplitude and phase so that $\mathbf{E}(t)=\sum E_n\cos(\omega_n t-k_n z+\phi_n)$.

When the pump is of low enough intensity, only spontaneous Raman scattering (spontaneous emission) or SE will take place. As pump intensity is increased, stimulated Raman scattering or SRS will occur. SRS can be divided into two categories: Raman generation and Raman amplification.

The Raman generator has been studied by numerous authors[4-14]. The result from these studies relevant to this work is the prediction that in certain cases, the generated Stokes radiation, or field, may be correlated with the pump during its growth from SE in the generator. By correlation, one means that fluctuations in the Stokes field correspond to fluctuations in the pump field. This is predicted to be the case for the 1) phase diffusion model and 2) both the chaotic and multimode models in the limit when the laser bandwidth, Γ_L, is larger than the Raman linewidth, Γ_R.

Raman amplification, although studied by an equally large number of authors[15-34] has been mostly theoretical, rather than experimental in nature. Numerous applications of Raman amplification however have been exploited. Cleanup of spatially poor quality pump lasers through Raman conversion[15-19], and access to high energy beams through the multiplexing of several pump lasers with a single Stokes beam in a Raman amplification medium[18-22] are two of the most common applications.

Early work on Raman amplification[3,23-29] using models derived from the phase diffusing and multimode models showed

that the amplified Stokes spectrum was always narrower than the pump spectrum below a critical pump intensity. Above this critical intensity, the Stokes spectrum approached or even equaled the pump spectrum in width. It was also discovered that the gain for broadband amplification was nonlinear and always less than the narrowband gain below the critical pump intensity. These two effects were attributed to dispersion in the Raman amplification medium and hence related to the spectral width of the pump. As pump intensity was increased above the critical intensity, broadband gain became independent of both pump bandwidth and dispersion, and consequently approached the narrowband value. Raymer et al.[3], using the phase diffusion model, predicted theoretically that the pump and Stokes fields may become correlated in phase, which leads to monochromatic gain. Lombardi et al.[30], later showed experimentally that the Stokes does indeed acquire the same phase as the pump.

Vokhnik et al.[31] and Stappaerts et al.[32] were the first authors to investigate the effects of correlation between the pump and injected Stokes seed on gain enhancement. These authors showed that when the two fields were perfectly correlated, the gain enhancement is a maximum and approaches the narrowband value. Both Agarwal[33] and Georges[34] using the chaotic model made the interesting prediction that when the pump linewidth is narrower than the Raman linewidth, and when the two beams are well correlated, gains which are

larger than the monochromatic gain are to be expected.

It appears that no single model for Raman scattering will describe every experimental situation and each researcher must decide which model will work for any given laser and each particular experiment. In Dr. Carlsten's lab a XeCl laser (described in chapter three) is used to do Raman scattering. This thesis results from a first attempt at describing the radiation from a XeCl laser and it's interaction with the Raman medium. A multimode-fixed-random-phase model is developed, and using this model, the effects of correlation, linewidth, and input pump intensity on the broadband gain are studied. Experiments are performed and experimental results are compared with the theoretical predictions of this model.

CHAPTER TWO

DERIVATION OF THE RAMAN SCATTERING EQUATIONS

Introduction

A Raman medium is one capable of coupling optical frequencies which differ by a vibrational, rotational, or electronic frequency. The body of the work presented in this thesis will be concerned with vibrational Raman scattering; thus a brief description is appropriate.

Raman scattering is a two photon processes. Physical insight into vibrational Raman scattering is obtainable with a simple model. Consider the three level molecule in Fig.1. When a pump photon of frequency ω_p (also referred to as ω_L) is absorbed by the molecule, a Stokes photon of frequency ω_s is emitted and the molecule is left vibrating at the difference frequency ω_{13}, where $\hbar\omega_{13}$ is the energy difference between the molecular levels one and three. This difference frequency is referred to as the Raman shift.

A theoretical description of Raman scattering is considerably more complicated since both Schrodinger's equation and Maxwell's equations must be used. A feel for the theoretical approach may be obtained by referring to the block diagram in Fig.2. The interaction between the pump and Stokes fields in the medium is described by

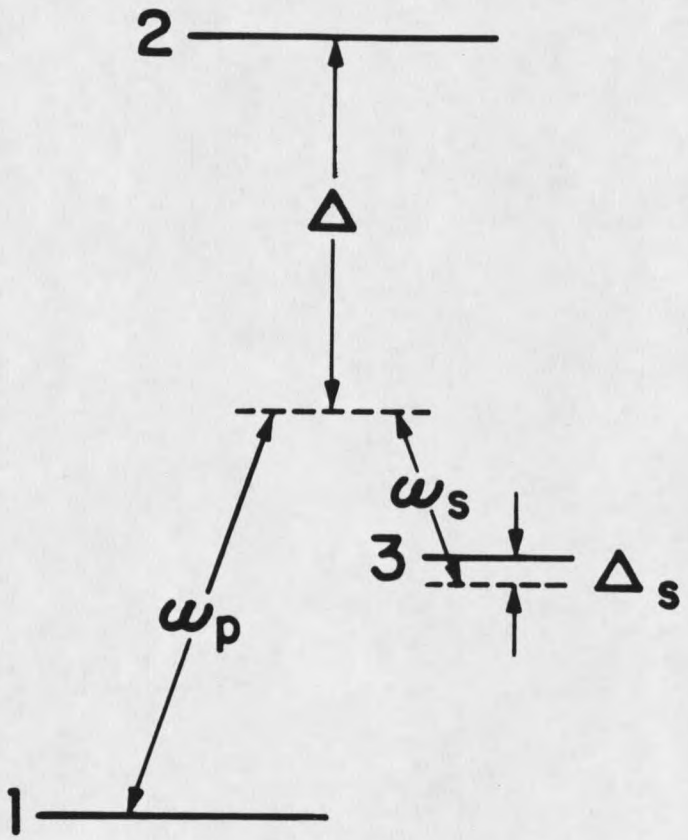

Figure 1. Energy level diagram for stimulated Raman scattering. A three level molecule interacts with a pump photon of frequency ω_p and a Stokes photon of frequency ω_s. The molecule is left vibrating at the difference frequency ω_{13}.

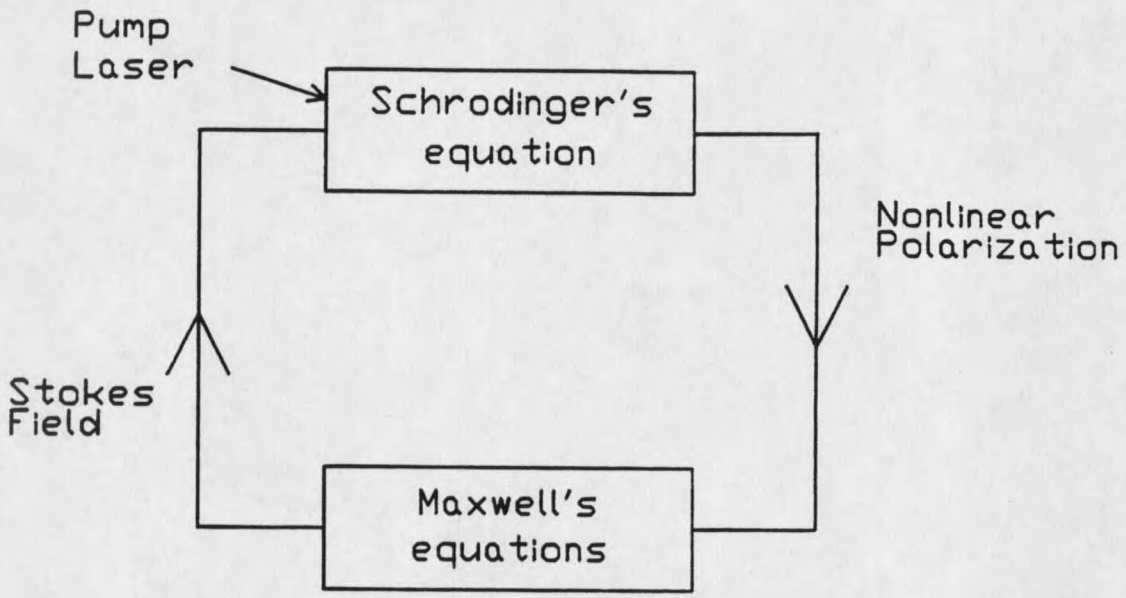

Figure 2. Self consistency diagram for stimulated Raman scattering. The pump and Stokes fields interact via Schrodinger's equation and produce a non-linear polarization in the medium. The non-linear polarization then drives the Stokes field via Maxwell's equation.

Schrodinger's equation. A nonlinear polarization in the medium results from this interaction and becomes the driving term in Maxwell's wave equation. The nonlinear polarization completely describes the macroscopic response of the medium to the incident fields, while Maxwell's wave equation completely describes the response of the fields to the medium. The remainder of this section will be devoted to the details of this process.

Response of the Medium

One begins by writing out the wave function for a system of three level molecules (described in chapter three) interacting with a laser field of frequency $\hbar\omega_L$ and a Stokes field of frequency $h\omega_S$. An energy level diagram for the system is shown in Fig.1 Following Raymer et al[3] we let

$$\Psi = a_1 \exp^{-i\Phi_1} U_1 + a_2 \exp^{-i(\Phi_1+\Phi_L)} U_2 + a_3 \exp^{-i(\Phi_1+\Phi_L-\Phi_S)} U_3 . \quad (1)$$

The a_i are the amplitudes of level i, Φ_i is equal to $\omega_i t - k_i z$ and the U_i are the stationary states having energies $\hbar\omega_i$. Since we are free to choose the zero of energy it is convenient to choose it to be the ground state with the phase, $\Phi_1 = 0$.

The Hamiltonian for the system is

$$H = H_0 + H' . \quad (2)$$

H_0 is the Hamiltonian for the unperturbed system having eigenvalues $E_i = \hbar\omega_i$, while H', the perturbing Hamiltonian describes the interaction of light with the system and is

given by the dipole interaction[35]

$$H' = \mu \cdot E = -ex\frac{1}{2}(E\exp i\Phi + c.c.). \tag{3}$$

We let the system evolve by putting ψ into Schrodinger's equation, $i\hbar\dot{\psi}=H\psi$. This yields

$$\begin{aligned} i\hbar(a_1 U_1 + [a_2 - ia_2\omega_L]\exp^{-i\Phi_L} U_2 \\ + [a_3 - ia_3(\omega_L-\omega_S)]\exp^{-i(\Phi_L-\Phi_S)} U_3) \\ = Va_1U_1 + (\hbar\omega_2+V)a_2\exp^{-i\omega_L t}U_2 \\ + (\hbar\omega_3+V)a_3\exp^{-i(\omega_L-\omega_S)t}U_3. \end{aligned} \tag{4}$$

Perturbing the system with H' creates the probability of finding populations in excited states. The amplitude for populating excited states is determined by evaluating

$$i\hbar\langle\psi|\dot{\psi}\rangle = \langle\psi|H|\psi\rangle. \tag{5}$$

Collecting terms proportional to U_1 we obtain

$$i\hbar\dot{a}_1 = V_{11}a_1 + V_{12}a_2\exp^{-i\Phi_L} + V_{13}a_3\exp^{-i(\Phi_L-\Phi_S)}. \tag{6}$$

The dipole interaction only couples adjacent states, therefore $V_{11}=V_{13}=0$, and Eqn.6 simplifies to,

$$i\dot{a}_1 = -\Omega_{12}a_2 \tag{7}$$

where the Rotating Wave Approximation (RWA)[35] has been used and $\Omega_{ij}=eX_{ij}E/2\hbar$ is the Rabi frequency[36]. Similarly, we find

$$i\dot{a}_2 = \Delta_L a_2 - \Omega_{21}^{*}a_1 - \Omega_{23}^{*}a_3 \tag{8}$$

and

$$i\dot{a}_3 = a_3\Delta_S - \Omega_{32}a_2. \tag{9}$$

$\Delta_L=\omega_2-\omega_L$ describes how far the laser is tuned from the resonant 1-2 transition and is assumed to be very large for the purposes of this derivation (see appendix A), while

$\Delta_S=\omega_3-(\omega_L-\omega_S)$ is the detuning for the Raman transition and assumed to be negligibly small.

Determination of the population $|a_i|^2$ of level i requires the simultaneous solution of the system of equations 7, 8, and 9. It is convenient to solve Eq.8 first. Integrating both sides of this expression yields

$$a_2(t) = \int_0^t G(t')\exp^{i\Delta_L(t'-t)}dt' \tag{10}$$

where $G(t')=i(\Omega_{12}^{*}a_1 + \Omega_{32}^{*}a_3)$.

Integrating by parts gives

$$a_2(t) = \frac{G(t) - G(0)\exp^{-i\Delta_L t}}{i\Delta_L} - \frac{G(t) - G(0)\exp^{-i\Delta_L t}}{(i\Delta_L)^2} - \frac{G(t) - G(0)\exp^{-i\Delta_L t}}{(i\Delta_L)^3} . \tag{11}$$

The second and third terms in this expression will be small compared to the first term for large Δ_L and can be ignored. At t=0, $a_1(0)=1$ and $a_2(0)=a_3(0)=0$ so that $G(0)=-i\Omega_{12}^{*}a_1$. Thus

$$a_2(t) = \frac{(\Omega_{12}^{*}a_1 + \Omega_{32}^{*}a_3)}{\Delta_L} - \frac{\Omega_{12}^{*}a_1\exp^{-i\Delta_L t}}{\Delta_L} . \tag{12}$$

For large Δ_L, the second term will be oscillating very fast compared to the first term and can be ignored so that

$$a_2(t) \approx \frac{(\Omega_{12}^{*}a_1 + \Omega_{32}^{*}a_3)}{\Delta_L} . \tag{13}$$

This is tantamount to $\dot{a}_2\approx 0$. These approximations conveniently reduce the three level problem to a two level

problem; the system can be considered to be oscillating between levels 1 and 3 only.

Rewriting equations 7 and 9 with the expression for a_2 given by Eq.13 we obtain

$$\dot{a}_1 = \frac{i(|\Omega_{12}|^2 a_1 + \Omega_{12}\Omega_{32}^* a_3)}{\Delta_L} \tag{14}$$

and

$$\dot{a}_3 = \frac{i(\Omega_{32}\Omega_{12}^* a_1 - |\Omega_{32}|^2 a_3)}{\Delta_L}. \tag{15}$$

Again, rather than solving these two simultaneous equations it is expedient to introduce the density matrix formulation[35] by defining

$$Q^* = 2a_1^* a_3 \tag{16}$$

where Q^* is related to the off diagonal density matrix elements and has the physical interpretation of a coherence between the states a_1 and a_2. Additionally, with this formulation it is possible to include the effects of collisions between molecules in the medium. The effect of collisions is to introduce dephasing between the ground and excited states which in turn destroys the coherence between these states. The time evolution of the coherence is given by

$$\frac{\partial Q^*}{\partial t} = 2(\dot{a}_1^* a_3 + a_1^* \dot{a}_3) - \Gamma Q^* \approx \frac{i2\Omega_{32}\Omega_{12}^*}{\Delta_L} - \Gamma Q^* \tag{17}$$

or

$$\frac{\partial Q^*}{\partial t} = -\Gamma Q^* + ik_1 E_S E_L^* \quad \text{with } k_1 = \frac{d_{12}d_{23}}{2\Delta_L \hbar^2} \tag{18}$$

where terms proportional to a_3 have been assumed small and neglected , collisional dephasing is accounted for by the inclusion of the damping term Γ, and the d_{ij} are the matrix elements $e\langle U_i|X|U_j\rangle$. Eq.18 tells us that the pump and Stokes fields create coherence in the medium and collisions between molecules destroy it. Eq.18, then describes the microscopic response of the medium to the applied fields.

The macroscopic response of the medium is manifest in the polarization which is given by

$$P_{ij} = N\langle\psi_i|\mathbf{d}\cdot\mathbf{X}|\psi_j\rangle + c.c. \qquad (19)$$

where $\mathbf{d}\cdot\mathbf{X}$ is the dipole moment per unit volume and N is the number of dipoles contained within the volume. The component of the polarization which drives the Stokes field is given by

$$P_{23} = N\langle\psi_2|\mathbf{d}\cdot\mathbf{X}|\psi_3\rangle + c.c. \qquad (20)$$

With the wave function given by Eq.1 along with Eq.13 and Eq.16 the polarization can be written in terms of the coherence Q^*, yielding

$$P_{23} = Nd_{23}(\Omega_{21}Q^*\exp^{i\Phi}S + \Omega_{21}^*Q^*\exp^{-i\Phi}S). \qquad (21)$$

So, using the pump and Stokes fields in Schrodinger's equation we have created a polarization in the medium, and thus completely described the macroscopic response of the medium to the applied fields.

Response of the Field

The polarization drives the Stokes field via Maxwell's

wave equation whose derivation follows. We begin with Maxwell's equations[37]

$$\text{I. } \nabla \times \mathbf{E} = -\frac{\partial \mathbf{B}}{\partial t} \qquad \text{II. } \nabla \times \mathbf{H} = \mathbf{J} + \frac{\partial \mathbf{D}}{\partial t} \qquad \text{III. } \nabla \cdot \mathbf{D} = \rho$$

and Ohm's law

$$\text{IV. } \mathbf{J} = \sigma \mathbf{E}$$

along with the relations

$$\text{V. } \mathbf{B} = \mu \mathbf{H} \qquad \text{VI. } \mathbf{D} = \varepsilon_0 \mathbf{E} + \mathbf{P}$$

and the vector identity

$$\text{VII. } \nabla \times \nabla \times \mathbf{A} = (\nabla \cdot \mathbf{A}) - \nabla^2 \mathbf{A}.$$

Substituting V. into I. and taking the curl of both sides results in

$$\nabla \times \nabla \times \mathbf{E} = -\mu \frac{\partial (\nabla \times \mathbf{H})}{\partial t} .$$

Applying the identity VII. and substituting IV. and VI.

$$(\nabla \cdot \mathbf{E}) - \nabla^2 \mathbf{E} = -\mu\sigma \frac{\partial \mathbf{E}}{\partial t} - \mu\varepsilon_0 \frac{\partial^2 \mathbf{E}}{\partial t^2} - \mu \frac{\partial^2 \mathbf{P}}{\partial t^2}. \tag{22}$$

The polarization is now separated into linear and nonlinear parts, that is, $\mathbf{P}=\mathbf{P}_L+\mathbf{P}_{NL}$. The linear polarization is given by[37] $\mathbf{P}_L=\varepsilon_0 \chi_L \mathbf{E}$, so that Eq.22 can be rewritten

$$\nabla^2 \mathbf{E} - (\nabla \cdot \mathbf{E}) - \mu\sigma \frac{\partial \mathbf{E}}{\partial t} - \mu\varepsilon \frac{\partial^2 \mathbf{E}}{\partial t^2} = \mu \frac{\partial^2 \mathbf{P}_{NL}}{\partial t^2} \tag{23}$$

where $\varepsilon=(1+\chi_L)\varepsilon_0$ is the permittivity[37] of the medium having a linear susceptibility χ_L. For wave propagation in gaseous media, there are no free charges which means that both the conductivity σ, and the divergence of $\mathbf{E}$ can be taken to be

zero.

Then, writing $\mu\varepsilon$ as $1/v^2$, Eq.23 simplifies

$$\nabla^2 E_S - \frac{1}{v^2}\frac{\partial^2 E_S}{\partial t^2} = \frac{4\pi}{c^2}\frac{\partial^2 P_{23}}{\partial t^2} \tag{24}$$

where the Stokes field E_S has been substituted for E, the polarization from Eq.21 has been substituted for P_{NL}, and a transformation to Gaussian units[38] has been made.

Equations 18 and 24 are sufficient to describe stimulated Raman scattering, though Eq.24 is more commonly written as a first order differential equation and in a slightly different form. This transformation will be derived next.

Considering propagation in the z direction only, the Stokes field can be written

$$E_S = \frac{1}{2}(E_S \exp^{i\Phi S} + c.c.) \tag{25}$$

where $\Phi_S=\omega_S t-k_S z$ and E_S is complex with a slowly varying phase. Substituting this field into the left side of Eq.24 yields

$$-ik_S \exp^{i\Phi S}\, \bar{D}E_S + c.c. \tag{26}$$

where the Slowly Varying Envelope Approximation[36] (SVEA) has been evoked, and D is the differential operator defined by

$$\bar{D} = \frac{\partial}{\partial z} + \frac{1}{v}\frac{\partial}{\partial t}. \tag{27}$$

Writing out the complex exponential as a real and imaginary term, and letting $\alpha=DE$ and $\alpha^*=DE^*$, the expression given by

26 can be rewritten

$$-ik_S\left[(\alpha-\alpha^*)\cos\Phi_S + i(\alpha+\alpha^*)\sin\Phi_S\right] . \qquad (28)$$

Similarly, the right side of Eq.24 can be written

$$-\frac{2\pi N d_{23}\omega_S^2}{c^2\Delta_L}\left[(\beta+\beta^*)\cos\Phi_S + i(\beta-\beta^*)\sin\Phi_S\right] \qquad (29)$$

where $\beta=\Omega_{12}Q^*$, $\beta^*=\Omega_{12}^*Q$, and SVEA was again invoked. But now note, for any complex number $\gamma=x+iy$,

$$x = Re\gamma = \frac{\gamma+\gamma^*}{2} \qquad \text{and} \qquad y = Im\gamma = \frac{\gamma-\gamma^*}{i2} \qquad (30)$$

so that

$$Im\bar{D}E\cos\Phi_S + Re\bar{D}E\sin\Phi_S = \frac{-N2\pi\omega_S v_S d_{23}}{c^2\Delta_L}(Re\Omega_{12}Q^*\cos\Phi_S - Im\Omega_{12}Q^*\sin\Phi_S). \qquad (31)$$

Using the results of Eq.30, Eq.31 can be written as

$$\bar{D}E = -ik_2Q^*E_L \quad \text{with } k_2 = \frac{N\pi\Omega\omega_S v_S d_{12} d_{23}}{\hbar c^2\Delta_L}. \qquad (32)$$

Eq.32 is the complete wave equation for the Stokes field. It tells us that spatial and temporal changes in the propagation of the Stokes field are driven both by the coherence and the pump laser. It should be noted that an equivalent expression to Eq.32 can also be written for the pump field, but this is of no interest in the present work, which is concerned only with the evolution of the Stokes field.

In summary then, the two equations, 18 and 32, give a complete description of the problem. They describe, as

promised, the response of the medium to the applied fields and the response of the fields to the medium.

CHAPTER THREE

ACCOUTERMENTS

Equipment and Technique

Spatial profiles and interference patterns, discussed in the next section of this chapter, were digitized using an EG&G Reticon "G" series self-scanning linear photodiode array. The array uses 1024 photodiodes on 25μm centers. The arrays are typically encased by a glass window. Since glass strongly attenuates the UV and adds the additional complication of interference from its two surfaces, the arrays used in these experiments were specially ordered without windows.

The array collects light continuously and is cleared by a scan. Each scan is triggered by a read pulse and takes 4ms to complete. In practice, the array is triggered by an external source with a repetition rate of approximately .5Hz. To reduce the background arising from stray room light, the array is read twice. At the onset of the read pulse the array scans once which clears it and after a .2ms wait, scans again. The second scan is read either with a storage oscilloscope or with digitizing electronics which send the information directly to a computer for storage. When using the photodiode array to measure spatial profiles

of the excimer laser, a 4.2ms delay is introduced between the trigger and the laser to insure that the second scan begins after the arrival of the laser pulse.

Usually, the spatial profiles of interest are inordinately small in diameter and in utterly inaccessible locations e.g. inside of a Raman cell. In these not so special cases, an imaging technique developed by Dr. Carlsten was used. An f=10cm focal length lens is inserted in the beam, 12cm from the location of interest and the photodiode array is located at the image distance, 60cm from the lens. The photodiode array "sees" a magnified image of the beam 72cm from the point of interest.

An experimental measurement of the magnification was made using the apparatus shown in Fig.3. A 1mm aperture was placed in the attenuated laser beam which had been clipped "upstream" with a 4.5mm aperture to obtain a diffraction limited beam, as discussed in the next section. The photodiode array was initially placed immediately in front of the aperture and a measurement was made to confirm that the diameter of the aperture was 1mm. Next, the f=10cm lens was placed in the system and the aperture was imaged onto the array where another measurement was made. A digitized plot of the measured results are shown in figures 4a for the actual aperture and 4b for the image of the aperture. One calculates the magnification by simply taking the ratio of the image to object distance, which for this case is 5. The

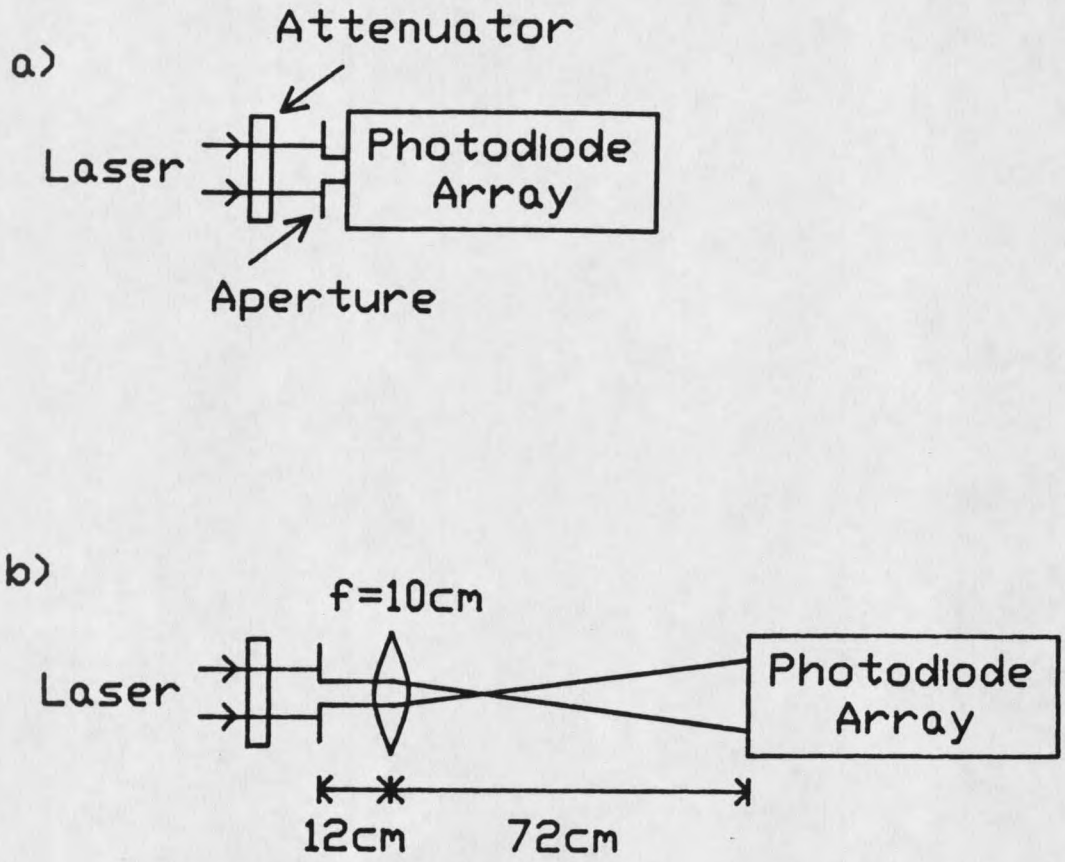

Figure 3. Schematic of experiment to measure the magnification of the f=10cm lens. The laser was attenuated with an appropriate dielectric filter and then clipped with a 1mm aperture. The aperture was first measured (a) with a photodiode array, and then (b) the image of the aperture was projected onto the array.

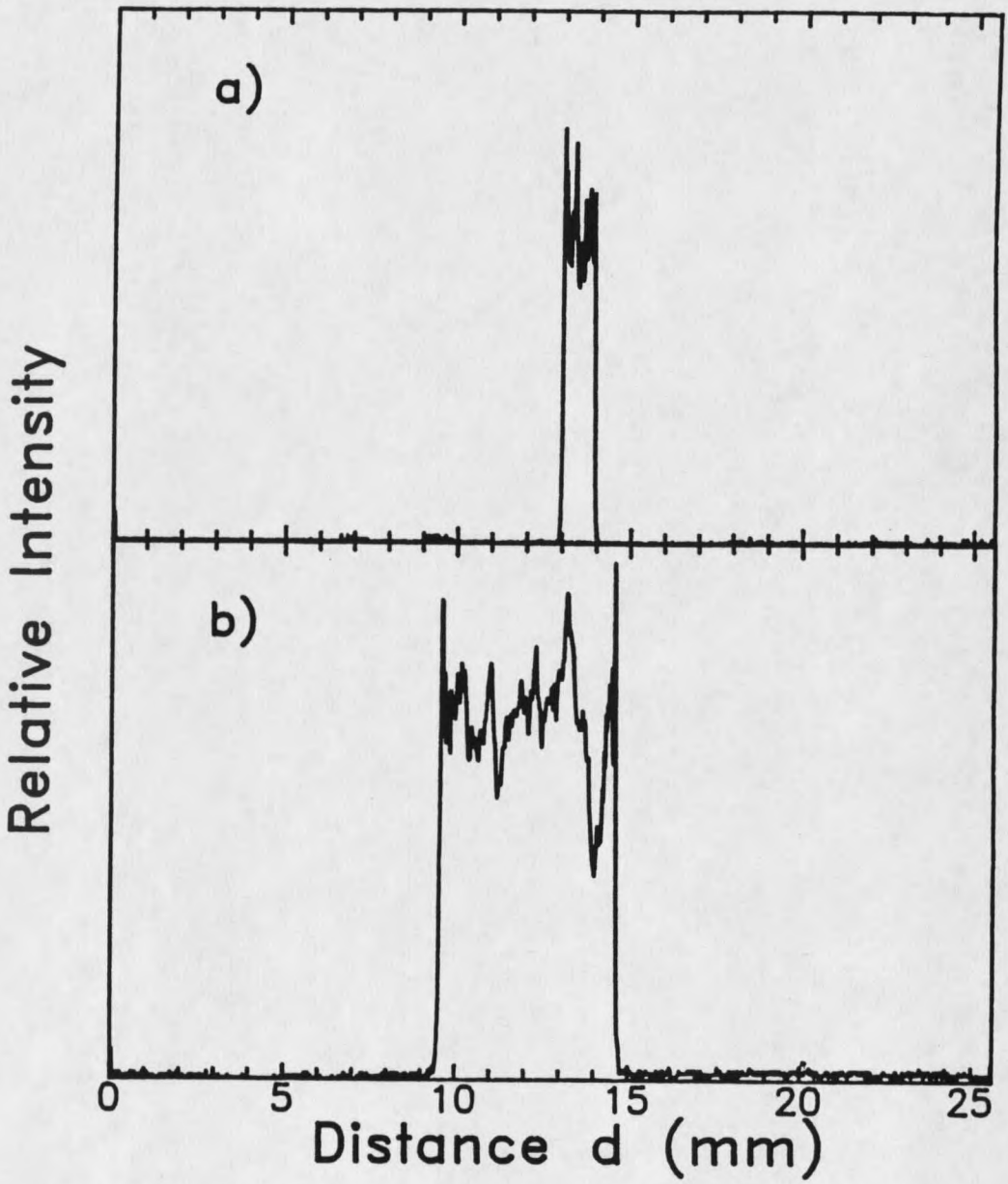

Figure 4. Digitized plot of (a) the aperture measured with the photodiode array and (b) the image of the aperture measured with the array.

experimentally measured value was 5.13.

Energy measurements were made with a Laser Precision Rj-7200 energy ratiometer, RjP-700 energy probe, and RjI serial to parallel interface. An HP-85 computer was interfaced to the forementioned electronics which were used in combination to collect the data.

In the next section, several plots of laser lines are shown. These lines were resolved with a Bausch and Lomb spectrograph which had a second order dispersion of 7.5 A/mm and second order spectral range of 1850-3700 angstroms. A photodiode array was placed at the output of the spectrograph and monitored with a Tektronix 2230 100MHz digital storage oscilloscope. The spectrograph, though inadequate as a device to accurately measure the width of each laser line, was immensely useful as a monitor of changes in linewidth during the course of an experiment.

The Laser

The laser used in this thesis work was an injection locked Lambda Physik EMG-150ET, which is a pulsed, gas discharge laser. A schematic of the laser is shown in Fig.5a. The laser uses an oscillator-amplifier configuration. The oscillator light, after passing through a number of intra-cavity Brewsters prisms becomes significantly narrowed and polarized to better than 90% in the horizontal. The light, after leaving the oscillator,

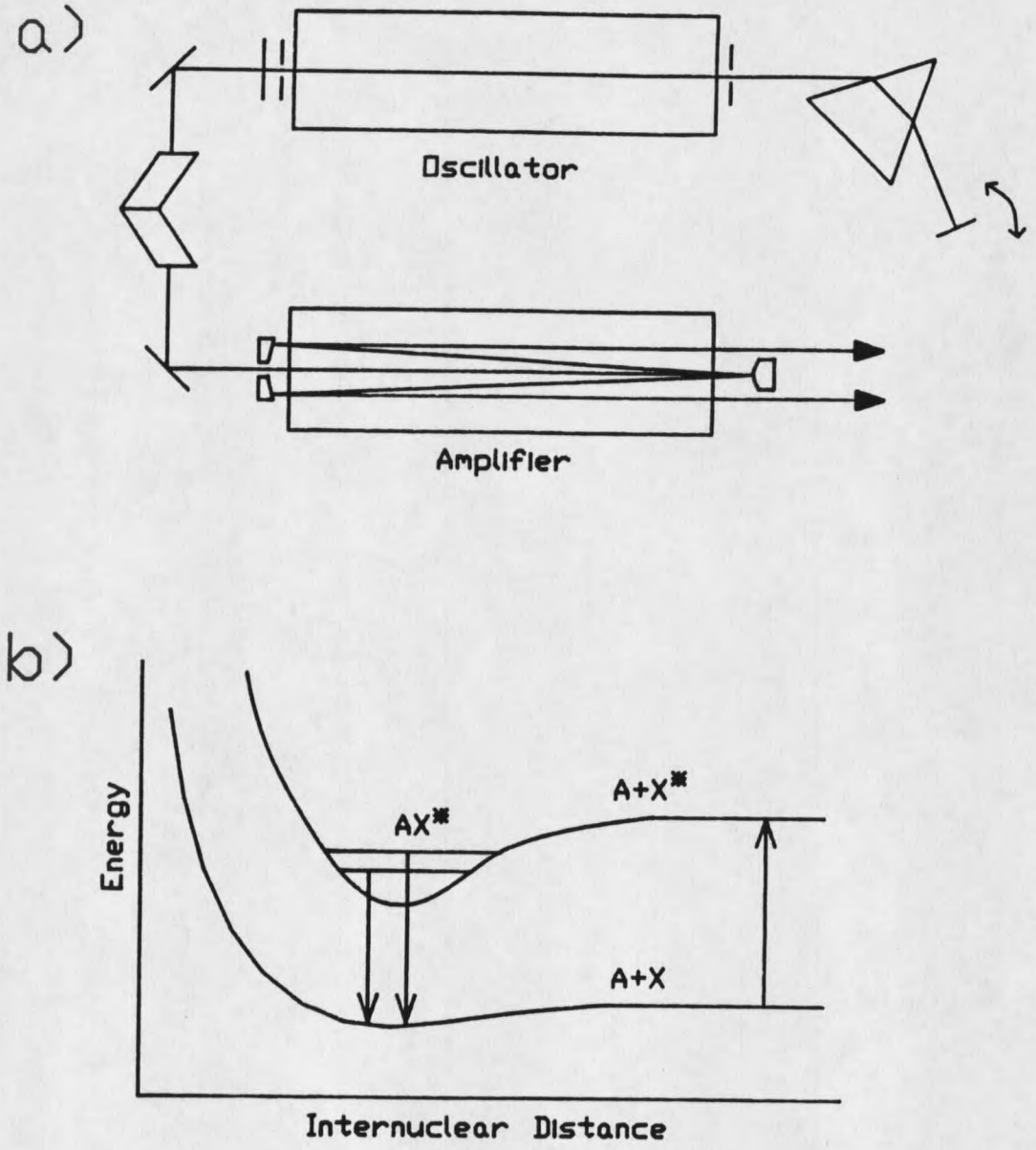

Figure 5. (a) schematic for the XeCl laser and (b) energy level diagram for the XeCl bond.

passes through two Fresnel rhombs which rotate the polarization from the horizontal into the vertical and then the light is injected into the amplifier, a three pass unstable resonator. The amplifier light becomes locked into the same vertical state of polarization as the injected oscillator light with an efficiency of better than 80%.

The laser's active medium, a gas, consists of the halogen gas, chlorine and the noble gas, xenon. Since xenon is inert, the ground state for the laser is repulsive and the molecules bond only in the excited state forming excimers[39] (molecules which exist only in the excited state). As is shown in Fig.5b, lasing only takes place on the transition between bound and unbound states with the ground state always empty. Thus, the excimer laser is considered to be very efficient.

According to the Lambda Physik catalog[40], the laser spectrum consists of four lines, two strong lines at 307.9nm and 308.15nm, and two weak lines at 307.6nm and 308.56nm, along with a weak subsidiary line at 308.2nm. Shown in Fig.6 is a plot of the digitized output from the spectrograph described in the previous section. As is shown in Fig.6a, we typically see only the 307.9nm, 308.1nm and 308.2nm lines. By tuning in the horizontal the rear mirror of the oscillator cavity, we are able to select to a certain degree which frequency light returns to the Brewster prisms at the appropriate angle for maximum transmission. Thus we

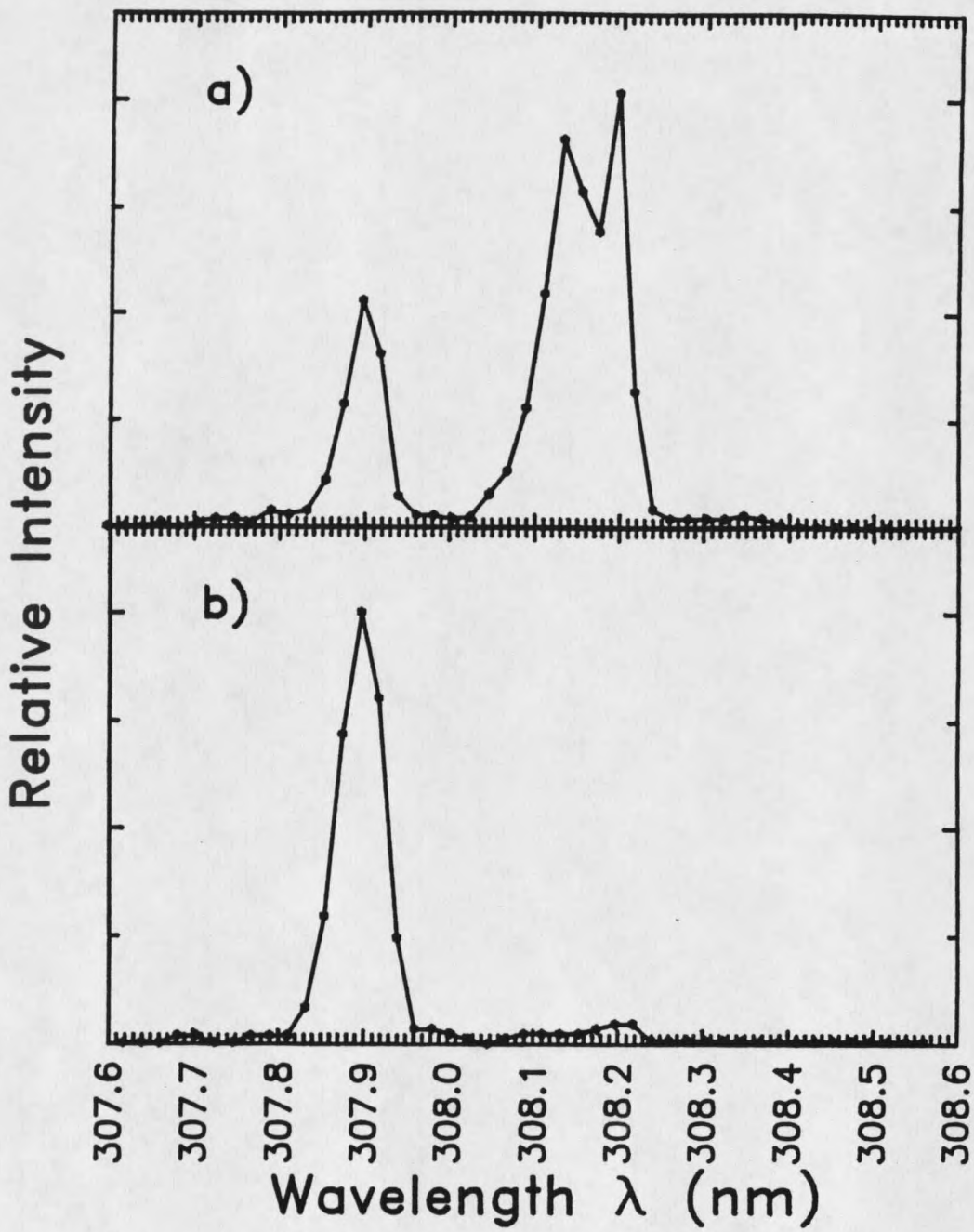

Figure 6. Digitized plot from the spectrograph showing (a) the three lines of the XeCl laser and (b) the result of tuning the laser on the 307.9nm line.

are able to tune between the three lines. We chose to tune the laser on the 307.9 line and as is shown in Fig.6b, in doing so, suppress the other two.

The temporal profile of the laser was measured with a Hamamatsu R1193U-02 phototube and a Tectronix 7834 500MHz storage oscilloscope. A digitized plot of the temporal profile is shown in Fig.7. By approximating the pulse as rectangular with a height equal to the peak power and an area equal to the total energy, the pulse width was calculated and equal to 15.3ns.

A measurement was also made of the laser linewidth. To make this measurement, a Mach-Zehnder interferometer shown schematically in Fig.8 was constructed. The path length of one beam was varied relative to the other using a three mirror corner-cube mounted on a linear motor drive which was originally constructed for the gain enhancement experiment discussed in chapter 6.

The output of the interferometer, was a series of interference profiles or interferograms. Each interferogram was for a different path length difference and was recorded with a linear photodiode array. An example of an interferogram is shown by the solid line in Fig.9.

The interference fringes are described by the irradiance function41 which is defined as

$$I(x) = I_1 + I_2 + 2(I_1 I_2)^{1/2} \mathrm{Re}\gamma(x). \qquad (33)$$

$\gamma(x)$ is the normalized autocorrelation function and is